Creep and Reliability Prediction of a Fan-Out WLP Influenced by the Visco-Plastic Properties of the Solder

Ramiro Sebastian Vargas Cruz[1] and Viktor Gonda[2]

[1]Óbuda University, Doctoral School on Materials Sciences and Technologies, Bécsi út 96/b, 1034 Budapest, Hungary
ramiro.vargas@stud.uni-obuda.hu

[2]Óbuda University, Donát Bánki Faculty Mechanical and of Safety Engineering, Népszínház u. 8, 1081 Budapest, Hungary
gonda.viktor@bgk.uni-obuda.hu

Abstract: Solder joint reliability is critical in the design of advanced microelectronic packaging. Predictions of reliability by thermo-mechanical simulations can accelerate the evaluations of advanced packaging and the introduction of novel solder materials. In this work, a finite element model of a thermally loaded Fan-Out Wafer Level Package (FO-WLP) was built and analyzed focusing on the creep behavior of the solder balls and the consequent effect on the reliability of the package. The lead-free soldering materials in the analyses were either of a widely used SAC305, or novel doped SAC solders as SAC-R, SAC-Q and InnoLot. Visco-plastic (Anand creep) properties for the solders were defined as study parameters, where 6 variations were used for the described SAC305, and further 3 sets for the doped SAC solders, respectively. Identifying a stress concentration at the sharp bond pad edges by modeling ideal geometries, a refined geometry was introduced and evaluated. Simulations for a 3-cycle thermal load were conducted, and results were collected and analyzed for Creep Strain and Strain Energies in critical positions in the solder, and reliability prediction was performed based on Morrow's model. Results show the benefit of the refined compositions of Doped SAC solders on the mechanical behavior and improved reliability.

Keywords: Reliability; Creep behavior; lead-free Solder

1 Introduction

The international pursuit of an environment free of hazardous substances and compliance with international regulations has undoubtedly affected how technology developed during the last years. According to the application, the allowed percentage of lead, cadmium, and other composites in electronic devices has been limited [1]. One of the most prevalent materials in microelectronic interconnects is

the solder alloy, which mechanically and electronically connects the components to the substrate [2]. Therefore, lead-free tin (Sn) based soldering materials have taken the market based on their similar performance to the eutectic tin-lead (SnPb) solder [3].

Simultaneously, the relentless technological development has looked for more compact electronic devices. Integrated Circuits (IC) are part of several applications, like the automotive industry, where the components undergo harsh environments and high temperatures [4]. Therefore, it is imperative to assure a reasonable lifetime of every element of the electronic board. This work aims to analyze the structural behaviour of an advanced microelectronic package by finite element simulations. A thermally loaded Fan-Out Wafer Level Package (FO-WLP) was modelled and analyzed focusing on the creep behavior of the solder balls and the consequent effect on the reliability of the package. The lead-free soldering materials in the analyses were either of a widely used SAC305, or novel doped SAC solders as SAC-R, SAC-Q and InnoLot. Visco-plastic (Anand creep) properties for the solders were defined as study parameters, where 6 variations were used for the described SAC305, and further 3 sets for the doped SAC solders, respectively. Simulations for a 3-cycle thermal load were conducted, and results were collected and analyzed for Creep Strain and Strain Energies in critical positions in the solder, and reliability prediction was performed. The outline of the paper is as follows: the Section 2 presents a concise introduction of electronic packaging. Subsequently, mathematical models that describe creep behavior and reliability for solders are presented. The section details the modelling approach, followed by a thorough analysis in the results and discussion sections.

2 Fan-Out Wafer Level Packaging (FO-WLP)

The electronic industry has been considered a crucial sector for technology development since the first working transistor was announced by AT&T (American Telephone and Telegraph) at Bell Laboratories. Hence, silicon-based transistors later developed by Texas Instruments resulted in a breakthrough with more reliable switching states [5]. Since 1970, Integrated Circuits (IC) have been part of the advancement in technologies and the computing industry. The chronological evolution of electronic packaging is detailed in Figure 1. The need for more efficient ICs constantly motivates the industry to increase the number of input/output (I/O) pins, while miniaturizing ICs.

During the last decade, Wafer Level Packaging (WLP) has been utilized to rapidly increase the number of I/O while reducing ICs size. Lau et al. [7] presented a concise review of the materials and trends regarding Fan-In and Fan-Out – WLP. Some of the advantages of WLP are a substrate-less package, lower thermal resistance, and higher performance due to shorter interconnects [8].

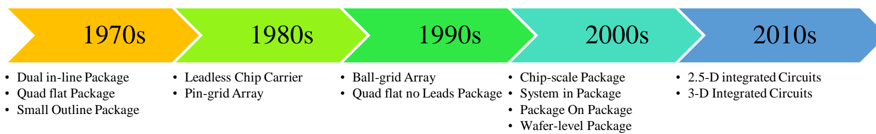

Figure 1
Evolution of semiconductor packaging [6]

Two basic Fan-Out WLP (FO-WLP) structures can be identified: Mold first and Redistribution Layer (RDL) first, based on the process flow (see Figure 2).

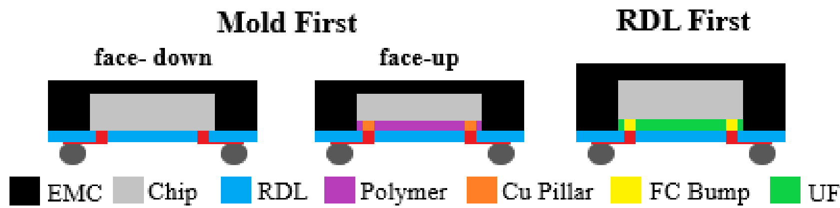

Figure 2
FO WLP Structures [9]
EMC: Epoxy Molding Compound, Cu: copper, FC Bump: Flip Chip Bump, UF: Underfill, and RDL: Redistribution Layer

Mold first – FO-WLP is already in mass production. Its advantage is related to the heterogeneous components needed in panels assemblies for energy harvest [9]. In addition, recent studies demonstrate that RLD first – FO-WLP could potentially replace some of the 3D ICs [10]. However, RDL first faces challenge to enhance wafer warpage and RDL scaling [11].

3 Solder Joint Modeling and Reliability

Reliability engineering has become a core part of all branches of industry. It consists of three main concepts (design for reliability DFR, reliability test & data analysis, and failure analysis) to effectively optimize the sources to predict failure [12]. The initial stage of reliability engineering (DFR) comprises the simulation procedure; once the optimal materials and measurements are manufactured in samples, reliability tests are conducted. The resulting data is then used for lifetime prediction. Finally, the failure analysis aims to understand the root cause based on faulty samples from the second stage. Recently, some standard tests for solder joint reliability have been identified. These tests usually imply endurance to changes in temperature, specific mechanical loads, and drop tests. Since creep behavior involves temperature, stress, and time, it has been implemented in several Finite Element Method (FEM) software packages [13]. The most common creep and reliability models are summarized in this section.

3.1 Anand Creep Model for Soldering Materials

Creep is time-dependent plastic deformation significant above half the absolute melting point [14]. Creep comprises three stages: primary, secondary, and tertiary. Along the primary stage (strain–hardening), the strain rate decreases as the hardening increases. Then, strain rate becomes constant; this is the steady-state creep. Finally, the strain rate rises exponentially in the tertiary stage, leading to a material fracture [15].

Mathematically, steady state creep behavior can be described by Norton Power Law [16], Garofalo-Arrhenius constitutive model [17], or Anand's constitutive model [18]. Norton's description is a basic approach that is refined in several subsequent work. The Garofalo-Arrhenius model has better accuracy [19] and extensively implemented in finite element software [20].

Anand [18] proposed two evolution equations from the flow equation (1) based on earlier theories suggested by Lee and Zaverl [21]. The primary purpose of this research was a better analysis of the deformation of metal alloys at elevated temperatures above $0.5T_m$ (absolute melting temperature). After a concice mathematical analysis on viscoplastic deformation at elevated temperatures, equations (2), (3), and (4) were finally proposed [22].

Flow equation:

$$\dot{\varepsilon}_p = A \cdot \exp\left(-\frac{Q}{RT}\right) \cdot \left(\sinh\left(\xi \frac{\sigma}{s}\right)\right)^{1/m} \quad (1)$$

where A is the pre-exponential factor, R is the universal gas constant, ξ is the multiplier of stress, s is the deformation resistance, and m is the strain rate sensitivity of stress.

Evolution equations:

$$B = 1 - \frac{s}{s^*} \quad (2)$$

$$\dot{s} = \{h_0 \cdot |B|^a \cdot \mathrm{sgn}(B)\}\dot{\varepsilon}_p \dot{s} = \{\mathrm{h_0}|\mathrm{B}|^{\mathrm{a}}\mathrm{sgn(B)}\}\dot{\varepsilon}_{\mathrm{p}} \quad (3)$$

$$s^* = \hat{s} \cdot \left(\frac{\dot{\varepsilon}_p}{A} \exp\left(\frac{Q}{RT}\right)\right)^n \quad (4)$$

where, s^* is the saturation resistance, h_0 is the hardening constant, a is the strain rate sensitivity of hardening, $\hat{s}$ is the deformation resistance saturation coefficient, and n is the strain rate sensitivity of saturation.

Anand model involves nine material parameters that can be determined following Brown's procedure [23]. Brown suggests at least two sets of three strain rate jump tests performed at different temperatures.

3.2 Failure Prediction Models

In ball grid array type packages, the Distance to Neutral Point (DNP) concept is widely employed to select critical solder joints [24]. The effectiveness of the DNP approach has been intensely discussed. Lau [25] stresses that DNP lifetime approximation presents some limitations. For instance, it was proven to be valid for packaging without underfill; however, it has been incorrectly applied on packaging with underfill [26]. The lifetime of the critical solder joint can be estimated by fatigue modells, such as the Coffin-Manson model based on strains, or the energy based Morrow's model among others.

3.2.1 Coffin-Manson Model

The Coffin-Manson model is strain-based analysis for low-cycle fatigue [27], where the equation is given as:

$$N_f \left(\Delta\varepsilon_p\right)^n = C \tag{5}$$

where, N_f is the predicted number of cycles to failure, n is the empirical constant, $\Delta\varepsilon_p$ is the inelastic strain range, and C is the proportionality factor/fatigue ductility coefficient.

According to Norris et al. [28], constant n was observed to be 2 for most metals. This mathematical approach has been widely studied. Zubelewicz et al. [29] stressed that the Coffin-Manson law does not fit experimental data well for high strain rates.

3.2.2 Morrow's Model

Morrow [30] proposed an energy-based equation to predict the number of cycles to failure:

$$N_f{}^{n'} W_p = A \tag{6}$$

where, n' is the fatigue exponent, A is the material ductility coefficient, and W_p is the inelastic strain energy density.

4 Simulation Procedure

This section thoroughly details the parameters for the electronic packaging simulations. First, the model's geometry, boundary conditions, and finally, the material properties are described. The simulations were carried out in Marc Mentat finite element software.

4.1 Geometry

For the finite element modeling, a 167GJJ Package from Texas Instruments [31] was selected. This FO-WLP package consists of a fine pitch Ball Grid Array (BGA). The main dimensions are shown in Figure 3.

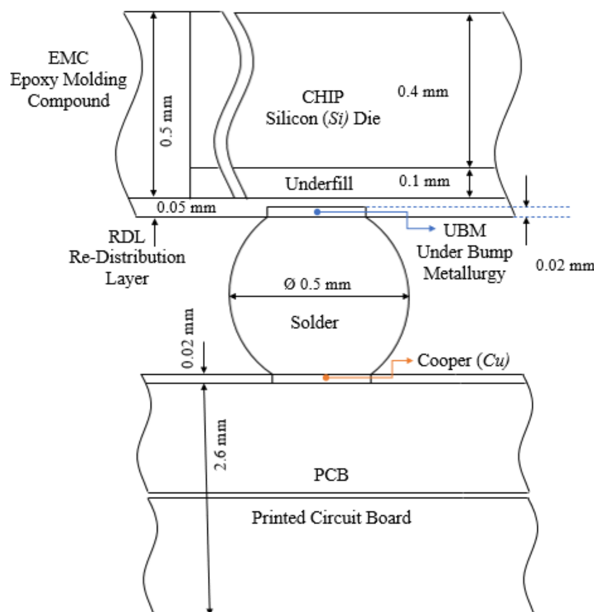

Figure 3
Main dimensions of the FO-WLP package section

The bottom copper layer was initially modeled with sharp pad edges considering an ideal geometry in previous works [32], [33]. However, during the processing, this edge may become blunt in real geometries. Therefore, a second variant is modeled using a fillet on the bottom copper layer. For simplicity, the model with the sharp-edged pad will be referred to as “squared” while the model with blunt-edged pads will be referred to as “rounded” (see Figure 4). Additionally, due to the complexity of the mesh, a mask layer was included in the squared model, whereas the same mask layer was excluded in the rounded model.

Two dimensional modelling was created to optimize the computing resources. Therefore, only half of the cross-section of the package was modeled. The complexity of the mesh utilized is not visible in Figure 4, the modeled layout is shown with the incorporated materials. The squared model was created using ruled mesh, while the rounded model was created using mesh seeds due to the fillet on the copper pad; the complete mesh contains over 200 000 elements and 115 000 nodes.

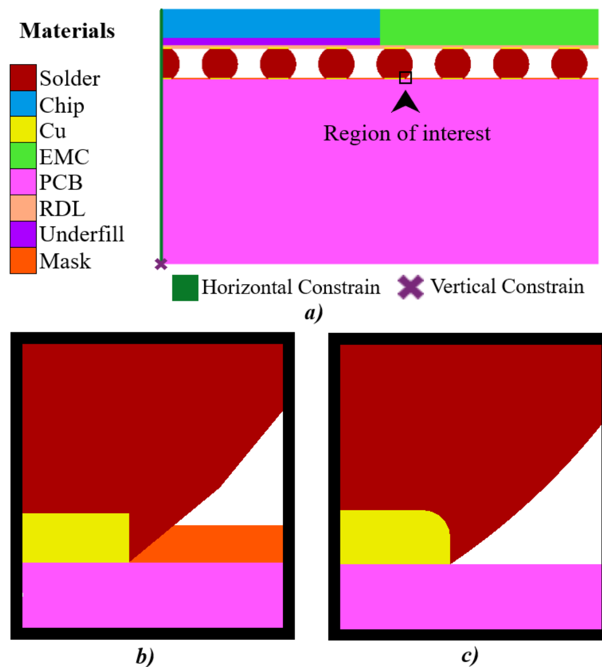

Figure 4
The modelled section: *a)* Materials description and boundary conditions, *b)* Augmented view of the squared Cu pad profile, and *c)* Augmented view of the rounded Cu pad profile

4.2 Initial and Boundary Conditions

A temperature of -40°C was set for all nodes for initial thermal conditions. For mechanical boundary conditions, mirror symmetry was considered by constraining the horizontal displacement on the model's left side. Constraints to vertical displacement were applied to the bottom left node for a unique solution (Figure 4). No extra mechanical loads were applied since the coefficient of thermal expansion mismatch will produce mechanical stress in the solder.

A cyclic thermal loading was applied to the modeled section. Previous studies on failure prediction have shown that a stable plastic work density is reached within three thermal cycles [34]. An average of strain and strain energy density can be computed, taking values at the second and third thermal cycles. Hence, a three-hour thermal load was applied to all the nodes in the model. The temperature ranged from -40°C to 125°C, as shown in Figure 5. This temperature range is in accordance with the Joint Electron Device Engineering Council (JEDEC) standards [35], and the maximum temperature surpasses $0.5T_m$. The repetitive cycle starts at -40°C, followed by a ramp-up that reaches 125°C within 15 minutes (heating stage).

Then, the temperature remains constant for the next 15 minutes, followed by a ramp-down that reaches -40°C in 15 minutes (cooling stage). Finally, the temperature is held for 15 minutes before the start of the next cycle.

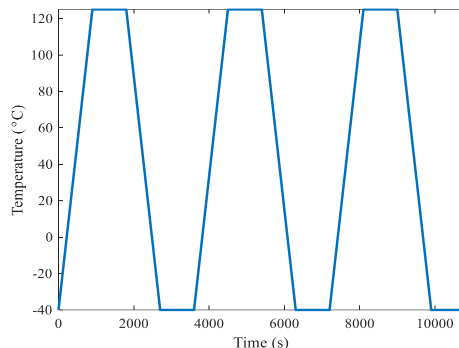

Figure 5
Thermal Load

In the finite element solver, a multi-criteria time stepping was selected for stable solutions with refined target step size, assuring the sufficiently large number of steps per cycle to maintain the accuracy of the calculations. Due to the fine mesh utilized for accurate results and small timesteps, the simulation process took about 8 hours for the squared profile and 6 hours for the rounded profile.

4.3 Material Properties

The material properties as Young's Modulus (E), Poisson's Ratio (υ), and Coefficient of Thermal Expansion (CTE) are summarized in Table 1 for the materials excluding the solder. These properties were considered time and temperature-independent, except for the Glass transition temperature (Tg) for certain materials. Under Bump Metallization (UBM) typically consist of Copper (Cu) coated with a noble metal to avoid corrosion, *e.g.,* Gold (Au) [36]. For simplification, the pad was modeled entirely of copper.

Table 1
Material Properties [37]

Material	***E* (GPa)**		***υ***	**CTE (ppm)**		**Tg* (°C)**
	T≤Tg	T>Tg		T≤Tg	T>Tg	
Chip	313		0.30	2.8		
Cu	117		0.34	17		
EMC	18.5	1.2	0.30	9	18	163
PCB	25		0.11	15		
RDL	0.92	0.1	0.30	80	227	205

Underfill	3.8	0.125	0.30	44	119	141
Mask	2.4	0.23	0.30	60	161	100

*Glass Transition Temperature

Table 2
Chemical composition (wt%) of the selected SAC solders

Solder	**Sn**	**Ag**	**Cu**	**Bi**	**Ni**	**Sb**
SAC-R [38]	96.62	0.00	0.92	2.46	0.00	0.00
SAC-Q [38]	92.77	3.41	0.52	3.30	0.00	0.00
InnoLot [38]	90.95	3.80	0.70	3.00	0.15	1.40
SAC305 [39]	95 – 96	3.8 – 4.2	0.3 – 0.7	0.00	0.00	0.00

Table 3
Anand Properties for the solder materials

	S_0 MPa	A s^{-1}	ξ -	m -	h_0 MPa	s MPa	n -	a -	Q $J\cdot mol^{-1}$
SAC305 from different experimental works									
Alam [41]	6.5	3700	4	0.47	70000	7.72	0.0315	1.9	95616.75
Basit [42]	21	3501	4	0.25	$180\cdot10^3$	30.2	0.01	1.78	77491.14
Herk. [43]	1.066	$1.43\cdot10^8$	1.472	0.14	5023.9	20.29	0.032	1.12	88581.38
Janz [44]	45.9	$5.87\cdot10^6$	2	0.09	9350	58.3	0.015	1.5	62026.17
Lall [45]	32.39	1100	6	0.39	174130	67.7	0.0008	1.75	33258
Mysore [46]	2.15	17.994	0.35	0.15	1525.98	2.53	0.028	1.69	82895.56
Doped SAC Solders									
SACQ [47]	0.405	$2.45\cdot10^8$	0.068	0.36	3521.56	0.638	0.0056	1.243	112313.8
SACR [38]	34.72	1000	6	0.15	145640	71.71	0.001	1.55	92290.52
InnoLot [38]	32.42	25000	7	0.35	88875	56.76	0.0097	1.45	89313.9

Four different lead-free Sn-Ag-Cu (Tin-Silver-Coper) type soldering materials were considered in this work; SAC305 and three doped SAC solders (SACX) (see Table 2). Temperature-dependent E and CTE were set for SAC305 (see Figure 6).

For creep modeling, several sets of Anand Parameters are available for SAC305 in the literature (Table 3), and Anand parameters for the SACX solders are summarized as well.

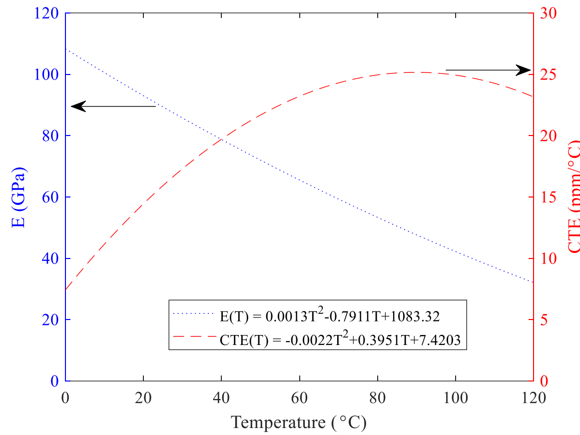

Figure 6
Temperature-dependent elastic modulus and CTE for SAC305 [40]

4.4 Overview of the Studied Cases

Alltogether, 11 cases are defined and summarized in Table 4. The main parameters were the material properties for the solder, and the solder pad geometry. The initial step was to compare the different sets of Anand parameters for SAC305 (Case 01 - 06). Next, a comparison between SAC305 and Doped SAC solders was carried out (Case 07 - 09). Once the results were analyzed, selected material properties were simulated with the round pad profile (Case 10 and 11).

Table 4
Summary of the main studied parameters

Case	Material	Edge Shape		Case	Material	Edge Shape	
		Sq.	Ro.			Sq.	Ro.
SAC305 Authors Comparison				Doped SAC Solders			
01	Alam	×		**07**	SACQ	×	
02	Basit	×		**08**	SACR	×	
03	Herkommer	×		**09**	InnoLot	×	
04	Janz	×		Edge shape comparison purposes			
05	Lall	×		**10**	Basit		×
06	Mysore	×		**11**	SACQ		×

Sq. = Squared, Ro = Rounded

5 Results and Discussion

The contour band graph of the Total Equivalent of Creep Strain (TECS) at the end of the simulation is shown in Figure 7. The node with the highest TECS is located on the outer bottom side of the solder ball. This result agrees with experimental data presented in [13], where in packaging including UBM cracking initiates in the bottom corners, while in packages without UBM cracking initiates in the upper corners. The magnified image in the bottom part of Figure 7 shows a significant change of the critical node location and the maximum value reached (0.22 for the squared profile and 0.09 for the rounded profile). The second most critical point occurred in the middle solder ball (4th from right to left on Figure 7). This result can be explained by the high number of materials in the vicinity of the solder ball. In addition, a mismatch of CTE increases the stress generated in the solder ball.

The levels of TECS in the upper side of the solder balls display a high concentration of strain under the EMC layer (see Figure 4 and Figure 7). Compared to experimental results, simulations on Wafer Level Chip Scale Package (WLCSP) support this phenomenon since solder crack initiated in the outer upper part of the solder ball [48].

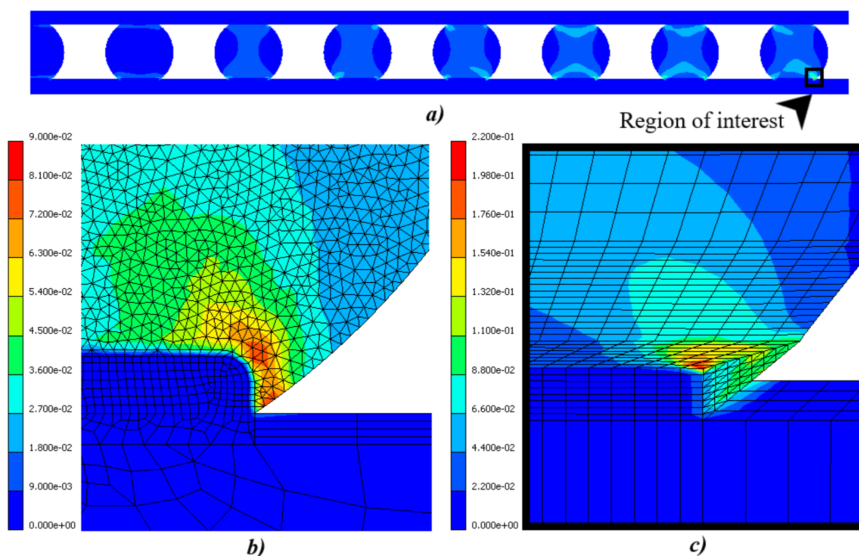

Figure 7

Total Equivalent of Creep Strain at the end of the three cycles: *a)* TECS distribution along the solder balls (cropped image), Augmented contour band graph of TECS distribution at the vicinity of the critical node *b)* rounded Cu pad profile and, *c)* squared Cu pad profile

5.1 Comparison of SAC305 Creep Parameters

TECS vs. time curves for the six sets of SAC305 Anand Parameters are plotted in Figure 8. The six replicates (study case 01 to 06) agreed on the most critical node location (outer bottom side of the solder ball as shown in Figure 7). There is a significant difference between the models of Mysore and Janz as compared to the rest of the Authors. Parameters of Alam, Basit, and Lall results in strains that are considerably similar. In terms of simulation time, the Basit parameters took significantly less time than Alam's and Lall's.

Although the six authors utilized the same composition, different experiments were followed to obtain Anand parameters. Shear stress and normal stress were measured and tabulated with shear strain and normal strain, respectively. The results displayed in Figure 8 cannot by established if the parameters are correct, but it can be a valuable tool for simulations where the time needs to be minimized. In such a case, Basit values approximate similar results to the remaining sets of Anand parameters while taking less time.

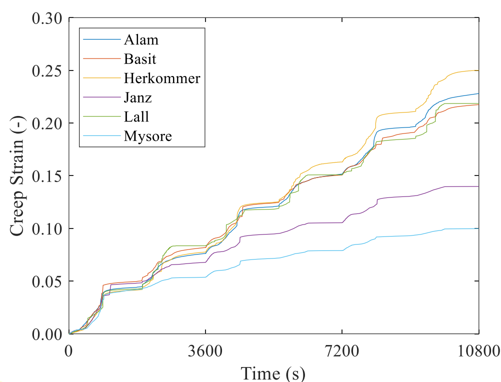

Figure 8

Total Equivalent of Creep Strain at the critical node – SAC305. Squared Profile

5.2 Comparison of SAC305 to Doped SAC Solders

Since the simulation using Anand parameters from Basit took less time to run, a second comparison was carried out between SAC305 (Basit) and Doped SAC solders. Creep Strain Energy Density (CSED) data was collected from the four replicates (case 02, 07 - 09). CSED vs. time curves are presented in Figure 9. According to Che and Pang [34], an approximation of the average of CSED can be computed taking values from the second and third thermal cycles. The obtained values were as follow: SAC305 = 0.2651 MPa; SACQ = 0.1627 MPa; InnoLot = 0.2550 MPa and SACR = 0.2019 MPa.

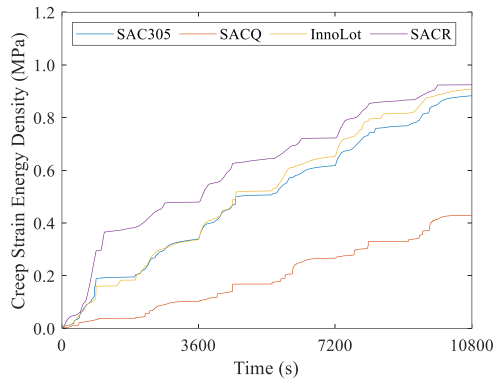

Figure 9

Creep Strain Energy Density SAC305 vs. Doped SAC Solders. Squared Profile

Based on Morrow's Model, presented in Section 3.2.2, the number of cycles to failure is inversely proportional to the average inelastic strain energy density. Therefore, in terms of CSED, SACQ would ideally perform longer than other Doped SAC solders and SAC305.

5.3 Effect of the Bond Pad Geometries

A comparison regarding the copper pad profile was carried out. Since the geometry of the modified model become too complex, the mask layer was neglected following similar study cases [49]. The fillet radius was assumed to be 20% of the copper pad width based on X-ray inspections taken from Lau [13].

Creeps strain curves (Equivalent of Creep Strain – ECS and TECS) from the critical node are presented in Figure 10. Like the squared profile, the location of the critical node remained the same.

The variation of change in profile within the same composition and between compositions are presented in Table 5. The column variations (Table 5) represent the difference of TECS between materials, while the row variations represent the variation due to the change in profile shape. It is clear to notice that in both compositions, the decrement due to shape is nearly 30%. On the other hand, a rounded profile accentuates the TECS difference between materials by 4.97%.

Regarding to Creep Strain Energy Density (CSED) and Total Strain Energy Density (TSED), curves are presented in Figure 11. In the case of SACQ, TSED for the squared profile presents several unstable peaks, and the general TSED values are not greater than those of CSED. On the other hand, TSED values are constantly greater than the CSED values for the rounded profile, and the curves follow a more stable pattern. In both cases, SAC305 and SACQ squared profile; the peaks show a time dependency and relaxation.

Table 5
TECS final value variation

	SAC305	**SACQ**	**variation**
Squared	0.0611	0.0463	**24.22%**
Rounded	0.0400	0.0323	**19.25%**
variation	**34.53%**	**30.23%**	

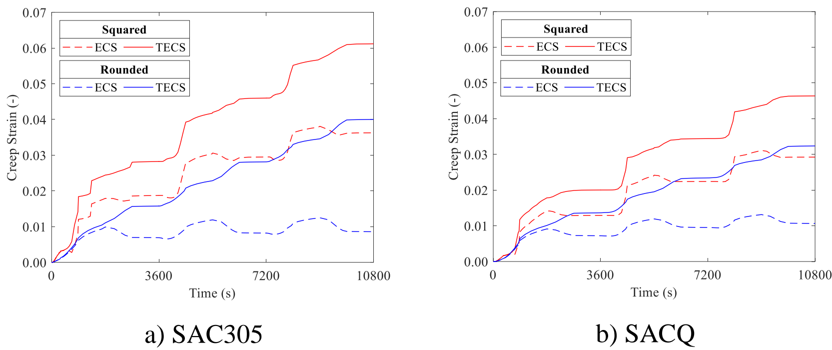

a) SAC305 b) SACQ

Figure 10
Creep Strain Curves

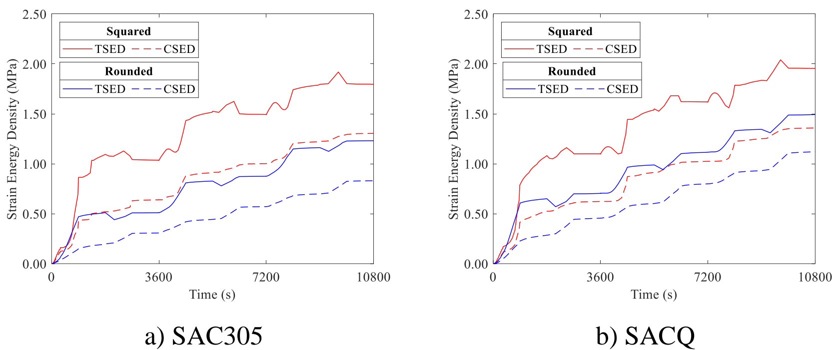

a) SAC305 b) SACQ

Figure 11
Strain Energy Density curves

CSED final values are summarized in Table 6. SAC305 reduced 31.45% due to a change in shape, while SACQ reduced 23.61%. It is interesting to see that the initial difference between materials was 8.11% using a squared profile. A change in profile increased the difference between materials to 17.54%. From Table 5 and Table 6, a change in the copper pad profile accentuates the variation of creep performance between materials.

Table 6

TSED final value variation

	SAC305	**SACQ**	**variation**
Squared	1.7960	1.9546	**8.11%**
Rounded	1.2311	1.4930	**17.54%**
variation	**31.45%**	**23.61%**	

5.4 Reliability Prediction Analysis

Following Che and Pang's procedure [34] (subtraction between final values of the third and second cycle), values of the approximation of average strain and energy variation were computed (see Table 7). It should be noted that all values decreased due to a change in copper pad geometry. High values can be observed for the squared profile with a significant reduction for the rounded profile. However, a more stable curve regarding TSED in SACQ (Case 11) increased inelastic strain energy density.

Table 7

Approximation of average of creep strain and energy density

	SAC305		**SACQ**	
	W_p	$\Delta\varepsilon_p$	W_p	$\Delta\varepsilon_p$
Squared	0.3028	0.0152	0.3347	0.0120
Rounded	0.3558	0.0119	0.3770	0.0090

Recent studies have reported Morrow and Coffin-Manson constants for estimation of the number of cycles to failure. It has been shown that the temperature, frequency, and aging may potentially affect the constants [50]. Morrow and Coffin-Manson constants for SAC305 and SACQ aging dependent have been reported in the last two years [51]. Nevertheless, temperature, and frequency dependency is needed for an accurate estimation using Table 7.

Conclusions

The reliability of the solder ball can compromise the functionality of the entire Integrated Circuit. Repetitive thermal loading of a complex FO-WLP package was modeled, varying the copper profile and solder ball material viscoplastic properties. Based on the results, the following conclusions can be drawn:

1) From the SAC305 comparison, six different sets of Anand Parameters were tested using simulation replicates. Not only the creep behavior was different, but also the simulation time. Basit parameters are suitable for simulation since it takes the minimum time, and the results do not significantly differ from the rest.

2) Since reliability models are inversely related to inelastic strain energy, SACQ presented the most promising working time, followed by SACR, Innolot, and SAC305 in that order.

3) A change in the copper pad profile shape (squared to rounded) shows a stress reduction and, therefore, more stable creep curves. Additionally, it accentuates the difference of creep values between materials by nearly 16% regarding creep strain values.

References

[1] European Parliament; The Council of The European Union, "Directive 2011/65/Eu of The European Parliament and of The CouncIL of 8 June 2011 on the restriction of the use of certain hazardous substances in electrical and electronic equipment (recast)," *Official Journal of the European Union*, 2011

[2] P. D. Sonawwanay and V. K. Bupesh Raja, "Eco-friendly Soldering Technique," in *Techno-Societal 2020*, Cham: Springer International Publishing, 2021, pp. 761-766

[3] J. Shepherd, "Lead Restrictions and Other Regulatory Influences on the Electronics Industry," in *Lead-Free Soldering*, J. Bath, Ed. Boston, MA: Springer US, 2007, pp. 5-19

[4] M. Traub, A. Maier, and K. L. Barbehon, "Future Automotive Architecture and the Impact of IT Trends," *IEEE Softw.*, Vol. 34, No. 3, pp. 27-32, May 2017, doi: 10.1109/MS.2017.69

[5] M. Riordan, "The lost history of the transistor," *IEEE Spectr.*, Vol. 41, No. 5, pp. 44-49, May 2004, doi: 10.1109/MSPEC.2004.1296014

[6] AnySilicon, "Semiconductor Packaging History and Trends," 2016. https://anysilicon.com/semiconductor-packaging-history-trends/

[7] J. H. Lau *et al.*, "Design, Materials, Process, Fabrication, and Reliability of Fan-Out Wafer-Level Packaging," *IEEE Trans. Components, Packag. Manuf. Technol.*, Vol. 8, No. 6, pp. 991-1002, Jun. 2018, doi: 10.1109/TCPMT.2018.2814595

[8] T. Braun *et al.*, "Opportunities of Fan-out Wafer Level Packaging (FOWLP) for RF applications," in *2016 IEEE 16th Topical Meeting on Silicon Monolithic Integrated Circuits in RF Systems (SiRF)*, Jan. 2016, pp. 35-37, doi: 10.1109/SIRF.2016.7445461

[9] T. Braun *et al.*, "Fan-Out Wafer and Panel Level Packaging as Packaging Platform for Heterogeneous Integration," *Micromachines*, Vol. 10, No. 5, p. 342, May 2019, doi: 10.3390/mi10050342

[10] L. T. Guan, C. K. Fai, and D. H. S. Wee, "FOWLP electrical performances," in *2016 IEEE 18th Electronics Packaging Technology Conference (EPTC)*, Nov. 2016, Vol. 3, pp. 79-84, doi: 10.1109/EPTC.2016.7861447

[11] V. S. Rao *et al.*, “Development of High Density Fan Out Wafer Level Package (HD FOWLP) with Multi-layer Fine Pitch RDL for Mobile Applications,” in *2016 IEEE 66th Electronic Components and Technology Conference (ECTC)*, May 2016, pp. 1522-1529, doi: 10.1109/ECTC.2016.203

[12] A. Birolini, *Reliability engineering: theory and practice*. Springer Science & Business Media, 2013

[13] J. H. Lau, “State of the Art of Lead-Free Solder Joint Reliability,” *J. Electron. Packag.*, Vol. 143, No. 2, Jun. 2021, doi: 10.1115/1.4048037

[14] M. E. Kassner, *Fundamentals of Creep in Metals and Alloys*. Elsevier, 2015

[15] G. Dieter, “Mechanical Metallurgy.” p. 615, 1961

[16] F. H. Norton, *The creep of steel at high temperatures*, No. 35, McGraw-Hill Book Company, Incorporated, 1929

[17] F. Garofalo and D. B. Butrymowicz, “Fundamentals of Creep and Creep-Rupture in Metals,” *Phys. Today*, Vol. 19, No. 5, pp. 100-102, May 1966, doi: 10.1063/1.3048224.

[18] L. Anand, “Constitutive Equations for the Rate-Dependent Deformation of Metals at Elevated Temperatures,” *J. Eng. Mater. Technol.*, Vol. 104, No. 1, p. 12, 1982, doi: 10.1115/1.3225028

[19] J. H. Lau, “Creep of 96.5Sn3.5Ag Solder Interconnects,” *Solder. Surf. Mt. Technol.*, Vol. 5, No. 3, pp. 45-52, Mar. 1993, doi: 10.1108/eb037839

[20] J. A. Depiver, S. Mallik, and E. H. Amalu, “Effective Solder for Improved Thermo-Mechanical Reliability of Solder Joints in a Ball Grid Array (BGA) Soldered on Printed Circuit Board (PCB),” *J. Electron. Mater.*, Vol. 50, No. 1, pp. 263-282, Jan. 2021, doi: 10.1007/s11664-020-08525-9

[21] D. Lee and F. Zaverl Jr, “A generalized strain rate dependent constitutive equation for anisotropic metals,” *Acta Metall.*, Vol. 26, No. 11, pp. 1771-1780, 1978

[22] L. Anand, “Constitutive equations for hot-working of metals,” *Int. J. Plast.*, Vol. 1, No. 3, pp. 213-231, 1985, doi: 10.1016/0749-6419(85)90004-X

[23] S. B. Brown, “An Internal Variable Constitutive Model for the Thixotropic Behavior of Metal Semi-Solid Slurries,” *Materials Science Seminar on Intelligent Processing of Materials*, Vol. 5. pp. 95-130, 1989

[24] T. C. Lui and B. N. Muthuraman, “Relibability assessment of wafer level chip scale package (WLCSP) based on distance-to-neutral point (DNP),” in *2016 22nd International Workshop on Thermal Investigations of ICs and Systems (THERMINIC)*, Sep. 2016, pp. 268-271, doi: 10.1109/THERMINIC.2016.7749063

[25] J. H. Lau, “The Roles of DNP (Distance to Neutral point) on Solder Joint

Reliability of Area Array Assemblies," *Solder. Surf. Mt. Technol.*, Vol. 9, No. 2, pp. 58-60, Dec. 1997, doi: 10.1108/09540919710800674

[26] W. Dauksher and W. S. Burton, "An examination of the applicability of the DNP metric on first level reliability assessments in underfilled electronic packages," *Microelectron. Reliab.*, Vol. 43, No. 12, pp. 2011-2020, Dec. 2003, doi: 10.1016/S0026-2714(03)00219-1

[27] S. S. Manson, "Thermal stress and low-cycle fatigue" 1966

[28] K. C. Norris and A. H. Landzberg, "Reliability of Controlled Collapse Interconnections," *IBM J. Res. Dev.*, Vol. 13, No. 3, pp. 266-271, May 1969, doi: 10.1147/rd.133.0266

[29] A. Zubelewicz, R. Berriche, L. M. Keer, and M. E. Fine, "Life-time prediction of solder materials," *Am. Soc. Mech. Eng.*, Vol. 111, No. September 1989, pp. 179-182, 1988

[30] J. Morrow, "Cyclic Plastic Strain Energy and Fatigue of Metals," in *Internal Friction, Damping, and Cyclic Plasticity*, 100 Barr Harbor Drive, PO Box C700, West Conshohocken, PA 19428-2959: ASTM International, 1965, pp. 45-87

[31] Texas Instruments Incorporated, "MicroStar BGA, Packaging Reference Guide," no. September. 2000

[32] R. S. Vargas C and V. Gonda, "Sensitivity of the structural behavior of SAC305 interconnects on the variations of creep parameters," May 2021, doi: 10.1109/SACI51354.2021.9465551

[33] R. S. Vargas Cruz and V. Gonda, "Solder joint reliability based on creep strain energy density for SAC305 and doped SAC solders," *MATEC Web Conf.*, Vol. 343, p. 02005, Aug. 2021, doi: 10.1051/matecconf/202134302005

[34] F. X. Che and J. H. L. Pang, "Thermal fatigue reliability analysis for PBGA with Sn-3.8Ag-0.7Cu solder joints," in *Proceedings of 6th Electronics Packaging Technology Conference (EPTC 2004) (IEEE Cat. No.04EX971)*, 2004, pp. 787-792, doi: 10.1109/EPTC.2004.1396715

[35] JEDEC Solid State Technology Association 2000, "JESD22-A104-B," *JEDEC STANDARD*, vol. Temperatur. Arlington, 2009 [Online] Available: http://web.cecs.pdx.edu/~cgshirl/Documents/22a104b Temperature Cycling.pdf

[36] Y. Degani, T. D. Dudderar, and K. L. Tai, "Flip chip packaging of memory chips." Google Patents, Nov. 23, 1999

[37] Z. Chen *et al.*, "Solder Joint Reliability Simulation of Fan-out Wafer Level Package (FOWLP) Considering Viscoelastic Material Properties," *2018 IEEE 20th Electron. Packag. Technol. Conf.*, pp. 573-579, 2019, doi: 10.1109/eptc.2018.8654355

[38] S. Ahmed, M. Basit, J. C. Suhling, and P. Lall, "Characterization of Doped SAC Solder Materials and Determination of Anand Parameters," in *Vol. 2: Advanced Electronics and Photonics, Packaging Materials and Processing; Advanced Electronics and Photonics: Packaging, Interconnect and Reliability; Fundamentals of Thermal and Fluid Transport in Nano, Micro, and Mini Scales*, Jul. 2015, pp. 1-14, doi: 10.1115/IPACK2015-48624

[39] K. Seelig and D. Suraski, "A COMPARISON OF TIN-SILVER-COPPER LEAD-FREE SOLDER ALLOYS," *Lead-free Solder Alloy.*, pp. 1-11, 2014

[40] T. T. Nguyen, D. Yu, and S. B. Park, "Characterizing the mechanical properties of actual SAC105, SAC305, and SAC405 solder joints by digital image correlation," *J. Electron. Mater.*, Vol. 40, No. 6, pp. 1409-1415, 2011, doi: 10.1007/s11664-011-1534-z

[41] M. S. Alam, K. M. R. Hassan, J. C. Suhling, and P. Lall, "High temperature mechanical behavior of SAC and SAC+X lead free solders," *Proc. - Electron. Components Technol. Conf.*, Vol. 2018-May, pp. 1781-1789, 2018, doi: 10.1109/ECTC.2018.00268

[42] M. Basit, M. Motalab, J. C. Suhling, and P. Lall, "Viscoplastic Constitutive Model for Lead-Free Solder Including Effects of Silver Content, Solidification Profile, and Severe Aging," in *Volume 2: Advanced Electronics and Photonics, Packaging Materials and Processing; Advanced Electronics and Photonics: Packaging, Interconnect and Reliability; Fundamentals of Thermal and Fluid Transport in Nano, Micro, and Mini Scales*, Jul. 2015, p. V002T01A002, doi: 10.1115/IPACK2015-48619

[43] D. Herkommer, J. Punch, and M. Reid, "Constitutive Modeling of Joint-Scale SAC305 Solder Shear Samples," *IEEE Trans. Components, Packag. Manuf. Technol.*, Vol. 3, No. 2, pp. 275-281, Feb. 2013, doi: 10.1109/TCPMT.2012.2227481

[44] D. T. Janz, "Reliability of discrete power devices with lead free solder joints." MS dissertation. Institute for Microsystem Technology, Albert Ludwigs …, 2004

[45] P. Lall, D. Zhang, and J. Suhling, "High strain rate properties of SAC305 leadfree solder at high operating temperature after long-term storage," in *2015 IEEE 65th Electronic Components and Technology Conference (ECTC)*, May 2015, pp. 640-651, doi: 10.1109/ECTC.2015.7159659

[46] K. Mysore, G. Subbarayan, V. Gupta, and Ron Zhang, "Constitutive and Aging Behavior of Sn3.0Ag0.5Cu Solder Alloy," *IEEE Trans. Electron. Packag. Manuf.*, Vol. 32, No. 4, pp. 221-232, Oct. 2009, doi: 10.1109/TEPM.2009.2024119

[47] T. C. Lui, "Life-time prediction of viscoplastic lead-free solder: A new solder material, SACQ," in *2017 IEEE International Workshop On Integrated Power Packaging (IWIPP)* Apr. 2017, pp. 1-4, doi: 10.1109/IWIPP.2017.7936754

[48] V. Ramachandran, K. C. Wu, and K. N. Chiang, "Overview Study of Solder Joint Reliablity due to Creep Deformation," *J. Mech.*, Vol. 34, No. 5, pp. 637-643, Oct. 2018, doi: 10.1017/jmech.2018.20

[49] Y. C. Chiou, Y. M. Jen, and S. H. Huang, "Finite element based fatigue life estimation of the solder joints with effect of intermetallic compound growth," *Microelectron. Reliab.*, Vol. 51, No. 12, pp. 2319-2329, 2011, doi: 10.1016/j.microrel.2011.06.025

[50] J. H. L. Pang, B. S. Xiong, and T. H. Low, "Low cycle fatigue models for lead-free solders," *Thin Solid Films*, Vol. 462-463, no. SPEC. ISS., pp. 408-412, 2004, doi: 10.1016/j.tsf.2004.05.037

[51] R. Al Athamneh, D. B. Hani, H. Ali, and S. Hamasha, "Reliability modeling for aged SAC305 solder joints cycled in accelerated shear fatigue test," *Microelectron. Reliab.*, Vol. 104, Jan. 2020, doi: 10.1016/J.MICROREL.2019.113507